STANFORD
AERONAUTICS &
ASTRONAUTICS

Transition in the Jet Created by an Impulsive Point Force

Brian Cantwell
Stanford University
May 23, 2025

STANFORD
AERONAUTICS &
ASTRONAUTICS

The jet created by an impulsively started point force

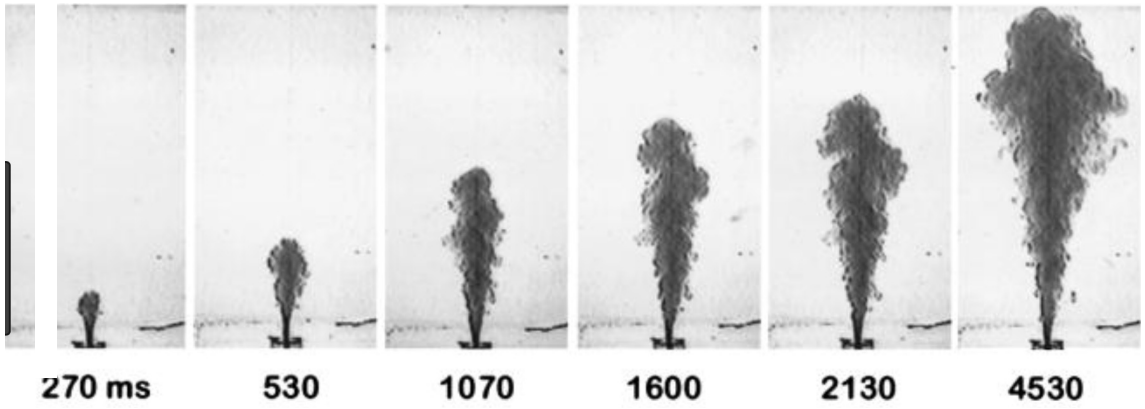

The usual situation is one where the jet is created by the flow of viscous fluid from a tube.

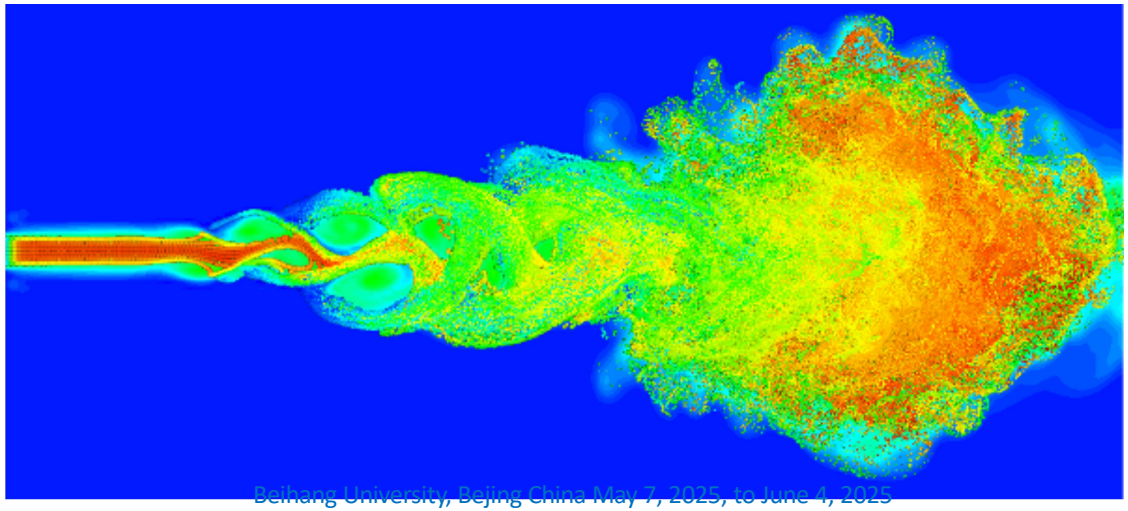

That is <u>not</u> quite the problem we are looking at. Our focus is on the jet produced by a point (zero length scale) force.

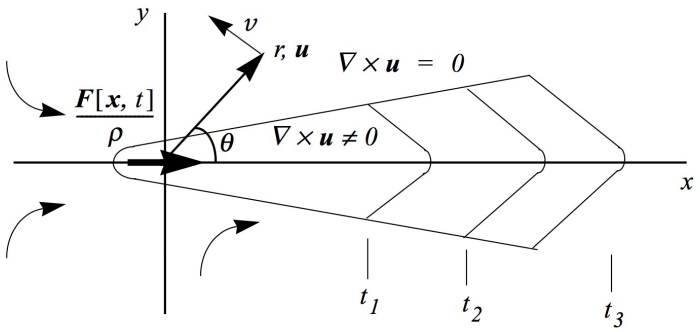

Fig. 11.4. Schematic of the unsteady propagation of a started jet. The boundary schematically delineates the regions of rotational and irrotational flow.

Figure 11.4 schematically shows the development of the vorticity-bearing region of an unsteady jet at several successive times. The jet is produced by a point force acting impulsively in a fluid that is initially everywhere at rest. The force distribution is of the form

$$\frac{\boldsymbol{F}[\boldsymbol{x},t]}{\rho} = \frac{J}{\rho} h[t]\delta[x]\delta[y]\delta[z]\,\hat{\mathbf{i}} \tag{11.75}$$

where $h[t]$ is the Heaviside function,

$$h[t] = \begin{cases} 0, & t < 0, \\ 1, & t > 0, \end{cases} \tag{11.76}$$

$\delta[x]$ is the Dirac delta function and J is the amplitude of the force directed along the x-axis. Using (11.57) and (11.73), the impulse integral is

$$\int_V \boldsymbol{u}[\boldsymbol{x},t]\,dx = \frac{2}{3}\left(\frac{J}{\rho}\right) t\,\hat{\mathbf{i}} \tag{11.77}$$

indicating that the total momentum of the fluid grows linearly with time.

STANFORD
AERONAUTICS &
ASTRONAUTICS

Governing equations

Equations of motion in spherical polar coordinates

$$\frac{1}{r}\frac{\partial(r^2 u)}{\partial r} + \frac{1}{\sin\theta}\frac{\partial(v\sin\theta)}{\partial\theta} = 0, \qquad \text{(continuity)},$$

$$\frac{\partial(rv)}{\partial r} - \frac{\partial u}{\partial\theta} = r\omega \qquad \text{(vorticity)},$$

$$\frac{\partial(r\omega)}{\partial t} + \frac{\partial(ru\omega)}{\partial r} + \frac{\partial(v\omega)}{\partial\theta} = \nu\left(\frac{1}{r}\frac{\partial}{\partial\theta}\left(\frac{1}{\sin\theta}\frac{\partial(\omega\sin\theta)}{\partial\theta}\right) + \frac{\partial^2(r\omega)}{\partial r^2}\right)$$

(momentum). (11.81)

Express the velocities in terms of the Stokes stream function

$$u = \frac{1}{r^2\sin\theta}\frac{\partial\psi}{\partial\theta}, \qquad v = \frac{-1}{\sin\theta}\frac{\partial\psi}{\partial r}. \tag{11.82}$$

Equations for particle paths

$$\frac{dr}{dt} = u[r,\theta,t], \qquad \frac{d\theta}{dt} = \frac{v[r,\theta,t]}{r}, \tag{11.83}$$

STANFORD
AERONAUTICS &
ASTRONAUTICS

Dilation symmetry group of the 3-D jet, k = 1/2

Now let's show that this problem is invariant under the fundamental dilation group of the Navier–Stokes equations,

$$\begin{aligned} \tilde{x}^i &= e^a x^i, & \tilde{t} &= e^{2a} t, \\ \tilde{u}^i &= e^{-a} u^i, & \frac{\tilde{p}}{\rho} &= e^{-2a} \frac{p}{\rho}, \\ \tilde{\omega} &= e^{-2a} \omega, & \tilde{\psi} &= e^a \psi. \end{aligned} \tag{11.78}$$

In spherical polar coordinates the transformation of the spatial coordinates is

$$\tilde{r} = e^a r \qquad \tilde{\theta} = \theta$$

Note that ψ in (11.78) is the Stokes stream function with dimensions $\hat{\psi} = L^3/T$. The invariance is confirmed by transforming the impulse integral

$$\begin{aligned} \int_V \tilde{\boldsymbol{u}}\, d\tilde{\boldsymbol{x}} = \frac{2}{3}\left(\frac{J}{\rho}\right)\tilde{t} \Rightarrow e^{2a}\int_V \boldsymbol{u}\, d\boldsymbol{x} &= e^{2a}\frac{2}{3}\left(\frac{J}{\rho}\right)t \\ \Rightarrow \int_V \boldsymbol{u}\, d\boldsymbol{x} &= \frac{2}{3}\left(\frac{J}{\rho}\right)t. \end{aligned} \tag{11.79}$$

The natural definition of the Reynolds number is

$$Re = \frac{(J/\rho)^{1/2}}{\nu}$$

$$\frac{\hat{J}}{\rho} = \frac{L^4}{T^2}, \quad k = \frac{1}{2}$$

independent of space and time.

STANFORD AERONAUTICS & ASTRONAUTICS

The characteristic equations of the group are

$$\frac{dr}{r} = \frac{d\theta}{0} = \frac{dt}{2t} = \frac{du}{-u} = \frac{dv}{-v} = \frac{d(p/\rho)}{-2p/\rho} = \frac{d\omega}{-2\omega} = \frac{d\psi}{\psi}. \quad (11.84)$$

All the relevant similarity variables are generated as integrals of (11.84).

$$\begin{aligned} \xi &= r/(\nu t)^{1/2}, \\ \theta &= \theta, \\ U[\xi,\theta] &= \frac{ut^{1/2}}{\nu^{1/2}}, \\ V[\xi,\theta] &= \frac{\nu t^{1/2}}{\nu^{1/2}}, \\ P[\xi] &= \left(\frac{p}{\rho}\right)\frac{t}{\nu}, \\ \Omega[\xi,\theta] &= \omega t, \\ \Psi[\xi,\theta] &= \frac{\psi}{\nu^{3/2}t^{1/2}}. \end{aligned} \quad (11.85)$$

STANFORD
AERONAUTICS &
ASTRONAUTICS

Upon substitution of (11.85), the equations of motion (11.81) become

$$\begin{aligned}
\frac{1}{\xi}\frac{\partial(\xi^2 U)}{\partial \xi} + \frac{1}{\sin\theta}\frac{\partial(V\sin\theta)}{\partial\theta} &= 0 \qquad \text{(continuity)},\\
\frac{\partial(\xi V)}{\partial\xi} - \frac{\partial U}{\partial\theta} &= \xi\Omega \qquad \text{(vorticity)},\\
\frac{\partial}{\partial\xi}\left(\left(U - \frac{\xi}{2}\right)\xi\Omega\right) + \frac{\partial(V\Omega)}{\partial\theta} &= \frac{1}{\xi}\frac{\partial}{\partial\theta}\left(\frac{1}{\sin\theta}\frac{\partial(\Omega\sin\theta)}{\partial\theta}\right)\\
&\quad + \frac{\partial^2(\xi\Omega)}{\partial\xi^2} \qquad \text{(momentum)},
\end{aligned} \tag{11.86}$$

and the self-similar velocities are

$$U = \frac{1}{\xi^2\sin\theta}\frac{\partial\psi}{\partial\theta}, \qquad V = \frac{-1}{\sin\theta}\frac{\partial\psi}{\partial\xi}. \tag{11.87}$$

The particle path equations (11.83) become

$$\frac{\partial\xi}{d\tau} = U[\xi,\ \theta; Re] - \frac{\xi}{2}, \qquad \frac{d\theta}{d\tau} = \frac{V[\xi,\ \theta;\ Re]}{\xi}, \tag{11.88}$$

where $\tau = \ln[t]$.

When recast in similarity coordinates, the particle path equations form an autonomous pair of 1st order ODEs with the jet Reynolds number as a parameter.

STANFORD
AERONAUTICS &
ASTRONAUTICS

Critical points in the vector field of particle paths

11.5.2.2 Critical Points in Three Dimensions

Much of the analysis that follows will focus on the various vector field patterns of (11.88) and on the critical points (ξ_c, θ_c); we have

$$\begin{aligned} U[\xi_c, \theta_c; Re] - \frac{\xi_c}{2} &= 0, \\ \frac{V[\xi_c, \theta_c; Re]}{\xi_c} &= 0, \end{aligned} \tag{11.89}$$

where the parametric dependence of the velocity field on the Reynolds number is indicated. One of the most important aspects of this approach is that structural features of the flow, which are not visible in the streamline pattern, become evident in the pattern of particle trajectories.

The analysis of the critical points of (11.88) is carried out using the theory developed in Chapter 3, Section 3.9.4. For this purpose it is easier to work with the particle path equations in Cartesian coordinates,

$$\frac{dx^i}{dt} = u^i(\boldsymbol{x}, t) \Rightarrow \frac{d\xi^i}{d\tau} = U^i[\boldsymbol{\xi}; Re] - \frac{\xi^i}{2}. \tag{11.90}$$

where $\xi^i = x^i/\sqrt{\nu t}$.

The character of a critical point is determined by expanding the flow in a Taylor series near the critical point and truncating at first order:

$$\frac{d\xi^i}{d\tau} = \left(A^i_j - \frac{1}{2}\delta^i_j\right)\Big|_{\boldsymbol{\xi}=\boldsymbol{\xi}_c} \left(\xi^j - \xi^j_c\right). \tag{11.91}$$

The similarity form of the velocity gradient tensor is

$$a^i_j = \frac{\partial u^i}{\partial x^j} = \frac{1}{t}\frac{\partial U^i}{\partial \xi^j} = \frac{1}{t}A^i_j[\boldsymbol{\xi}]. \tag{11.92}$$

Note that the value of the dimensioned velocity gradient tensor does not depend on J/ρ or ν. Therefore an observer moving at a fixed $\boldsymbol{\xi}$ can use the current value of the velocity gradient as a local clock to determine the global age of the flow, regardless of the flow Reynolds number.

The real solution of (3.175) is expressed as

$$\alpha_1 = a_1 + a_2, \tag{3.178}$$

and the complex (or remaining real) solutions are

$$\begin{aligned} \alpha_2 &= -\tfrac{1}{2}(a_1 + a_2) + \frac{i\sqrt{3}}{2}(a_1 - a_2), \\ \alpha_3 &= -\tfrac{1}{2}(a_1 + a_2) - \frac{i\sqrt{3}}{2}(a_1 - a_2). \end{aligned} \tag{3.179}$$

Solving (3.172) for the eigenvalues leads to the cubic discriminant

$$D = \tfrac{27}{4}R^2 + \left(P^3 - \tfrac{9}{2}PQ\right)R + Q^2\left(Q - \tfrac{1}{4}P^2\right). \tag{3.180}$$

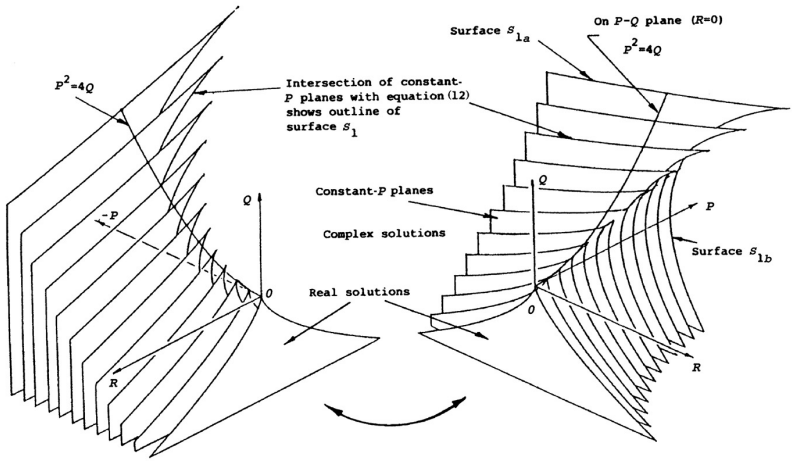

Fig. 3.8. The Cardano surface dividing real and complex eigenvalues in three dimensions (from Reference [3.10]).

Recall 3D critical points

3D Discriminant

$$D = \tfrac{27}{4}R^2 + \left(P^3 - \tfrac{9}{2}PQ\right)R + Q^2\left(Q - \tfrac{1}{4}P^2\right)$$

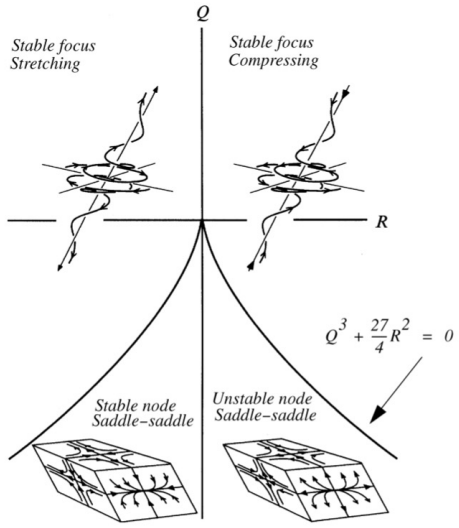

Fig. 3.9. Three-dimensional flow patterns in the plane $P = 0$ (from Reference [3.11]).

STANFORD AERONAUTICS & ASTRONAUTICS

The nature of the critical point is determined by the invariants of the matrix

$$M^i_j = A^i_j - \tfrac{1}{2}\delta^i_j \tag{11.93}$$

in (11.91) evaluated at the critical point. The first invariants of A and M are

$$P_M = \tfrac{3}{2}, \qquad P_A = 0. \tag{11.94}$$

The second and third invariants (Q, R) are expressed in terms of matrix elements

$$\begin{aligned} Q_A &= -\tfrac{1}{2}A^i_k A^k_i, \\ Q_M &= \tfrac{9}{8} - \tfrac{1}{2}M^i_k M^k_i \end{aligned} \tag{11.95}$$

and

$$\begin{aligned} R_A &= -\tfrac{1}{3}A^i_k A^k_j A^j_i, \\ R_M &= -\tfrac{1}{3}M^i_k M^k_j M^j_i - \tfrac{3}{2}Q_M + \tfrac{27}{24}. \end{aligned} \tag{11.96}$$

The invariants of M and A are related to one another as follows

$$\begin{aligned} Q_M &= Q_A + \tfrac{3}{4}, \\ R_M &= R_A + \tfrac{1}{2}Q_A + \tfrac{1}{8}. \end{aligned} \tag{11.97}$$

The discriminant of A is

$$D_A = Q_A^3 + \tfrac{27}{4}R_A^2, \tag{11.98}$$

and the discriminant of M is

$$D_M = Q_M^3 + \tfrac{27}{4}R_M^2 + \tfrac{27}{4}R_M\left(\tfrac{1}{2} - Q_M\right) - \tfrac{9}{16}Q_M^2. \tag{11.99}$$

If $D > 0$, the eigenvalues are complex and vorticity dominates the rate-of-strain. If $D < 0$, the eigenvalues are real and rate-of-strain dominates vorticity.

STANFORD
AERONAUTICS &
ASTRONAUTICS

For the axisymmetric flow considered here, the velocity gradient tensor takes the form

$$A^i_j = \begin{bmatrix} \dfrac{\partial U}{\partial \xi} & \dfrac{1}{\xi}\dfrac{\partial U}{\partial \theta} - \dfrac{V}{\xi} & 0 \\ \dfrac{\partial V}{\partial \xi} & \dfrac{1}{\xi}\dfrac{\partial V}{\partial \theta} + \dfrac{U}{\xi} & 0 \\ 0 & 0 & \dfrac{V}{\xi}\cot\theta + \dfrac{U}{\xi} \end{bmatrix}. \qquad (11.100)$$

Given the velocity functions, Equation (11.100) is evaluated at the critical point and the invariants are computed. Interestingly, it turns out that *often the values of the invariants can be determined without knowing the velocity functions explicitly*. In general, Q, R, ξ_c, and θ_c all depend on Re resulting in the possibility of bifurcation in the phase space of particle paths.

Boundary conditions for the impulsively started jet

11.5.2.3 The Limit $\xi \to 0$

Landau in 1944 [11.20] and, independently, Squire in 1951 [11.21] solved the steady problem of a jet emerging from a point source of momentum that was assumed to have been turned on for all time. The Stokes stream function for this case is

$$\psi = \nu r\left(\frac{2\sin^2\theta}{A[Re] - \cos\theta}\right). \tag{11.101}$$

The constant of integration, A, is related to the Reynolds number by considering an integral momentum balance over a sphere of fixed radius, R, enclosing the origin as shown in Figure 11.5.

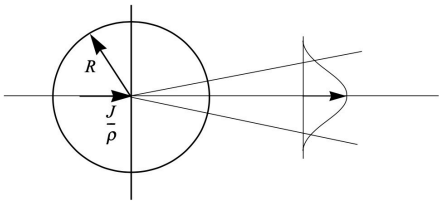

Fig. 11.5. Control volume surrounding the steady round jet.

Typical steady jet streamline pattern

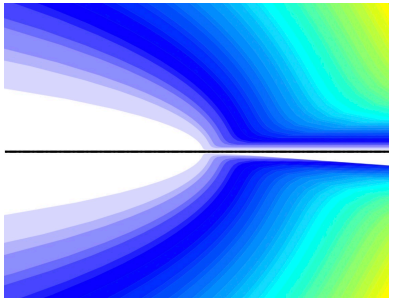

In this instance the rotational flow of the jet penetrates the control-volume surface, but the solution is known and the integration can be carried through. Balancing forces on the control volume leads to

$$\frac{J}{\rho} = \int_0^\pi (u(u\cos\theta - v\sin\theta) - \left(\frac{\tau_{rr}}{\rho}\cos\theta - \frac{P}{\rho}\cos\theta - \frac{\tau_{r\theta}}{\rho}\sin\theta\right) \times 2\pi R^2 \sin\theta\, d\theta. \tag{11.102}$$

The stresses are related to the velocity field by the usual Newtonian relations,

$$\frac{\tau_{rr}}{\rho} = \nu\left(2\frac{\partial u}{\partial r}\right), \qquad \frac{\tau_{r\theta}}{\rho} = \nu\left(r\frac{\partial}{\partial r}\left(\frac{v}{r}\right) + \frac{1}{r}\frac{\partial u}{\partial \theta}\right). \tag{11.103}$$

The pressure is related to the velocity field by the r and θ components of the momentum equation. In short, all the terms in (11.102) can be represented explicitly in terms of r, θ, and A, through repeated use of the Landau–Squire solution (11.101). When the integration is carried out, the result is

$$\frac{Re^2}{16\pi} = A + \frac{4}{3}\left(\frac{A}{A^2-1}\right) - \frac{A^2}{2}\ln\left(\frac{A+1}{A-1}\right). \tag{11.104}$$

This relation is plotted in Figure 11.6.

The solution (11.101) is a perfectly steady flow. However, we can put it in the unsteady self-similar form (11.85) by simply multiplying and dividing by $\sqrt{\nu t}$. We obtain the following limiting solution of the impulsively started jet near $\xi = 0$

$$\Psi_0 = \xi\left(\frac{2\sin^2\theta}{A[Re] - \cos\theta}\right). \tag{11.105}$$

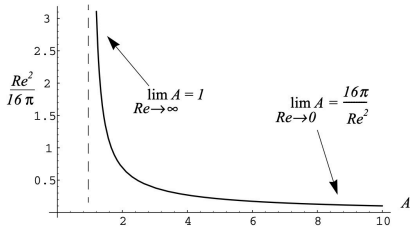

Fig. 11.6. The constant A in the Landau–Squire solution.

11.5.2.4 The Limit $\xi \to \infty$

In the previous section we examined Landau's solution for the steady jet cast in the form of an unsteady self-similar solution to the system (11.86). This solution conserves the flux of momentum from the source at $\xi = 0$, and at first glance there would seem to be no reason to go any further. However, we wish to consider a jet that has been turned on for a finite time and therefore has produced a flow field that contains a finite amount of momentum. The solution (11.105) violates this requirement. The flow at $\xi \to \infty$ must conserve momentum and be irrotational.

We have already worked out the vector potential at infinity when we worked out the impulse integral in Section 11.5.1. The Stokes stream function at infinity is

$$\psi = \frac{1}{4\pi}\left(\frac{J}{\rho}t\right)\frac{\sin^2\theta}{r}. \tag{11.106}$$

Here we replace $r \to \xi\sqrt{\nu t}$ and $J/\rho = Re^2\nu^2$. The limiting solution in the far field is

$$\Psi_\infty = \frac{Re^2}{4\pi}\left(\frac{\sin^2\theta}{\xi}\right). \tag{11.107}$$

The flow at infinity is that of a dipole of linearly increasing strength, Jt/ρ. This is also the total impulse applied to the fluid since the initiation of the momentum source (force) at the origin. As indicated in (11.57) and (11.73), two-thirds of this impulse is contained in the motion of the fluid directed along the jet axis, and one-third is lost to opposing unsteady pressure forces that act at infinity.

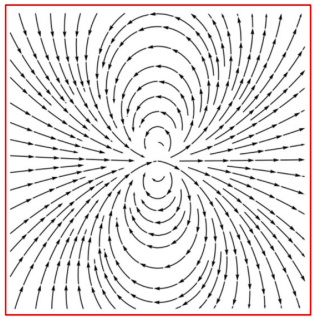

STANFORD
AERONAUTICS &
ASTRONAUTICS

$$\xi \to 0$$

11.5.2.6 Particle Paths of the Landau–Squire Jet

Now let's examine the flow pattern of the Landau–Squire solution, $\Psi_0[\xi, \theta]$. Using (11.87), substitute (11.105) into the particle-path equations in similarity coordinates (11.88). The result is

$$\frac{d\xi}{d\tau} = \frac{2}{\xi}\left(\frac{A^2-1}{(A-\cos\theta)^2} - 1\right) - \frac{\xi}{2}, \qquad \frac{d\theta}{d\tau} = \frac{2\sin\theta}{\xi^2(A-\cos\theta)}. \tag{11.115}$$

The system (11.115) has a single critical point on the axis of the jet, located at

$$(\xi_c, \theta_c) = \left(\frac{2^{3/2}}{(A-1)^{1/2}}, 0\right). \tag{11.116}$$

The relevant gradient tensors evaluated at the critical point are

$$A^i_j = \begin{bmatrix} -\frac{1}{2} & 0 & 0 \\ 0 & \frac{1}{4} & 0 \\ 0 & 0 & \frac{1}{4} \end{bmatrix}, \qquad M^i_j = \begin{bmatrix} -1 & 0 & 0 \\ 0 & -\frac{1}{4} & 0 \\ 0 & 0 & -\frac{1}{4} \end{bmatrix}, \tag{11.117}$$

and the invariants of M^i_j are $(P_M, Q_M, R_M) = (\frac{3}{2}, \frac{9}{16}, \frac{1}{16})$, independent of the Reynolds number. In the terminology of Reference [11.19], the critical point is a stable star node with three real negative eigenvalues, two of which are equal. As the Reynolds number is increased, the radial coordinate of the critical point increases although the invariants remain constant.

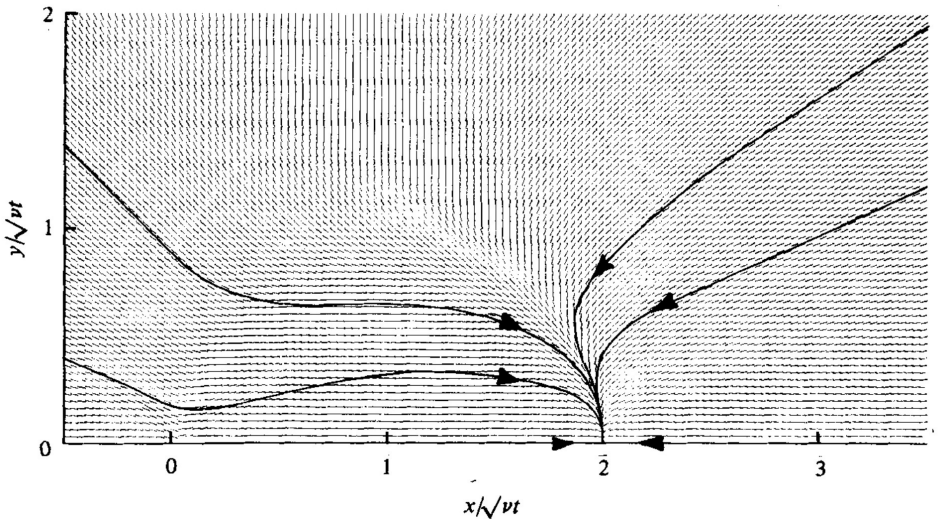

11.19 Chong, M. S., Perry, A. E., and Cantwell, B. J. 1990. A general classification of three-dimensional flow fields. *Phys. Fluids A* **2**(5):765–777.

STANFORD
AERONAUTICS &
ASTRONAUTICS

$$\xi \rightarrow \infty$$

11.5.2.7 *Particle Paths of the Unsteady Dipole*

The solution for the far field, (11.107), is substituted into (11.87) and (11.88), producing

$$\frac{d\xi}{d\tau} = \frac{Re^2}{2\pi}\frac{\cos\theta}{\xi^3} - \frac{\xi}{2}, \qquad \frac{d\theta}{d\tau} = \frac{Re^2}{2\pi}\frac{\sin\theta}{\xi^4}. \tag{11.118}$$

This system has a critical point on the jet axis at $(\xi_c, \theta_c) = (Re^{1/2}/\pi^{1/4}, 0)$. The two gradient tensors evaluated at the critical point are

$$A^i_j = \begin{bmatrix} -\frac{3}{2} & 0 & 0 \\ 0 & \frac{3}{4} & 0 \\ 0 & 0 & \frac{3}{4} \end{bmatrix}, \qquad M^i_j = \begin{bmatrix} -2 & 0 & 0 \\ 0 & \frac{1}{4} & 0 \\ 0 & 0 & \frac{1}{4} \end{bmatrix}, \tag{11.119}$$

and the invariants of M^i_j are $(P_M, Q_M, R_M) = (\frac{3}{2}, -\frac{15}{16}, \frac{1}{8})$. In the parlance of reference [11.19] the critical point is a node–saddle–saddle with three real eigenvalues: one negative, and two positive and equal. Here again, the invariants are independent of the Reynolds number, whereas the position of the critical point moves outward along the axis as the Reynolds number is increased.

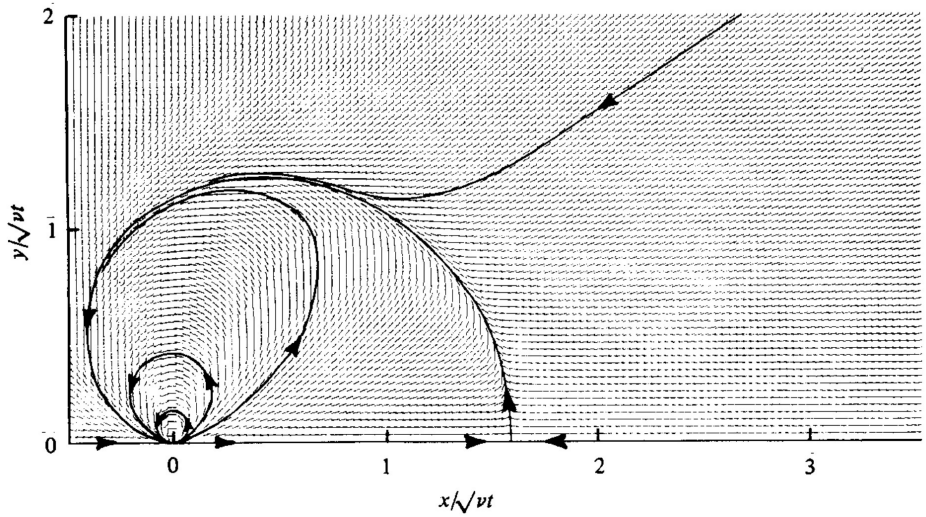

STANFORD
AERONAUTICS &
ASTRONAUTICS

The Stokes flow limit $Re \to 0$.

11.5.2.5 The Limit $Re \to 0$

If one takes the limit of (11.104) as $Re \to 0 (A \to \infty)$, the result is

$$A = 16\pi / Re^2. \tag{11.108}$$

In this limit the solution near $\xi = 0$ becomes symmetric in θ, and one can expect an overall solution of the form

$$\lim_{Re \to 0} \Psi[\xi, \theta] = \frac{Re^2}{16\pi} (\sin^2 \theta) g[\xi], \tag{11.109}$$

where the radial function must satisfy

$$\lim_{\xi \to 0} g[\xi] = 2\xi, \qquad \lim_{\xi \to \infty} g[\xi] = \frac{4}{\xi}. \tag{11.110}$$

Stream Function Re = 4

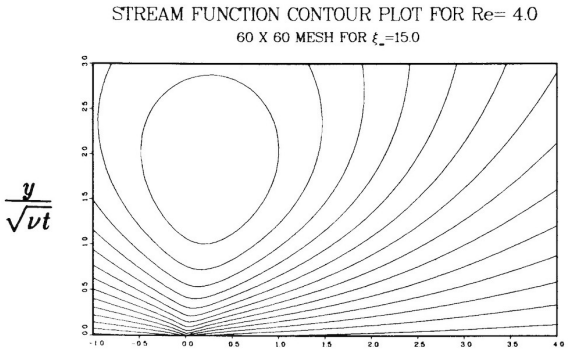

Vorticity Re = 4

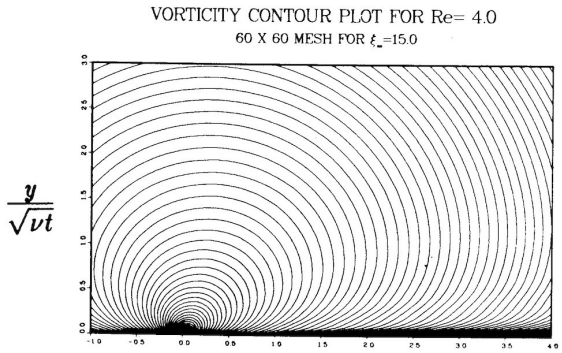

The corresponding vorticity is of the form

$$\lim_{Re \to 0} \Omega[\xi, \theta] = \frac{Re^2}{16\pi} (\sin^2 \theta) f[\xi]. \tag{11.111}$$

Equations (11.109) and (11.111) are substituted into (11.86), and higher-order terms in the small parameter $Re^2/16\pi$ are neglected. The result is the linear vorticity diffusion equation [the momentum equation in (11.81) with the non-linear terms removed]. Finally we end up with a linear second-order ODE governing the radial vorticity function $f[\xi]$:

$$\xi^2 f_{\xi\xi} + 2\xi \left(1 + \frac{\xi^2}{4}\right) f_\xi + (\xi^2 - 2) f = 0. \tag{11.112}$$

The radial parts of the vorticity function and stream function, f and g, are related through the definition of the vorticity,

$$\frac{d}{d\xi}\left(\frac{1}{\xi^2}\frac{d}{d\xi}(\xi g[\xi])\right) = -\frac{f[\xi]}{8}. \tag{11.113}$$

Equations (11.112) and (11.113) are solved using (11.110), leading to the solution of the Stokes creeping jet:

$$\lim_{Re \to 0} \Psi[\xi, \theta] = \frac{Re^2}{16\pi} \sin^2 \theta \left(2\xi - \frac{4}{\sqrt{\pi}} e^{-\xi^2/4} - \left(2\xi - \frac{4}{\xi}\right) \text{erf}\,[\xi/2]\right). \tag{11.114}$$

STANFORD
AERONAUTICS &
ASTRONAUTICS

Particle paths in the low Reynolds number jet

With that background we now consider particle paths of the low-Reynolds-number solution of the jet. Upon substitution of (11.114) into the particle-path equations (11.88) we have

$$\begin{aligned}\frac{d\xi}{d\tau} &= \frac{Re^2}{2\pi}\frac{\cos\theta}{\xi^2}\left(\frac{\xi}{2} - \frac{1}{\sqrt{\pi}}e^{-\xi^2/4} - \left(\frac{\xi}{2} - \frac{1}{\xi}\right)\operatorname{erf}[\xi/2]\right) - \frac{\xi}{2},\\ \frac{d\theta}{d\tau} &= -\frac{Re^2}{4\pi}\frac{\sin\theta}{\xi^2}\left(\frac{1}{2} + \frac{1}{\xi\sqrt{\pi}}e^{-\xi^2/4} - \left(\frac{1}{2} + \frac{1}{\xi^2}\right)\operatorname{erf}[\xi/2]\right).\end{aligned} \tag{11.120}$$

The critical points of (11.120) now need to be located. This is done by setting the right-hand sides equal to zero and solving for the roots. The zeros of the θ-equation occur at $\theta = 0,\ \pi$ for all ξ and at $\xi = 1.7633$ for all θ, independent of the Reynolds number. However, the zeros of the ξ-equation depend on Re as follows:

$$Re^2 = \frac{\pi\xi_c^3}{\left(\frac{\xi_c}{2} - \frac{1}{\sqrt{\pi}}e^{-\xi_c^2/4} - \left(\frac{\xi_c}{2} - \frac{1}{\xi_c}\right)\operatorname{erf}[\xi_c/2]\right)\cos\theta}. \tag{11.121}$$

STANFORD
AERONAUTICS &
ASTRONAUTICS

Particle paths in the Stokes jet at 3 Reynolds numbers

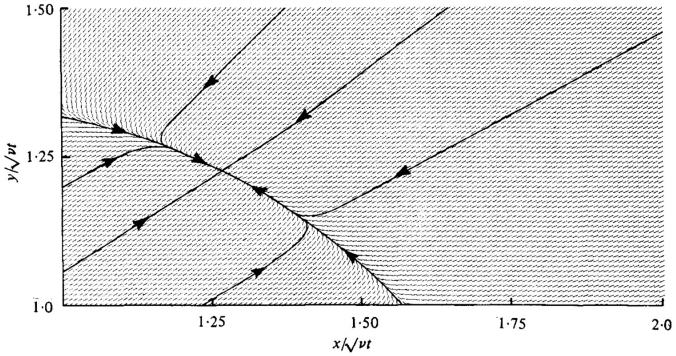

Transition in the jet created by an impulsive point force is in the nature of a sequence of bifurcations in the phase portrait of particle paths in similarity coordinates.

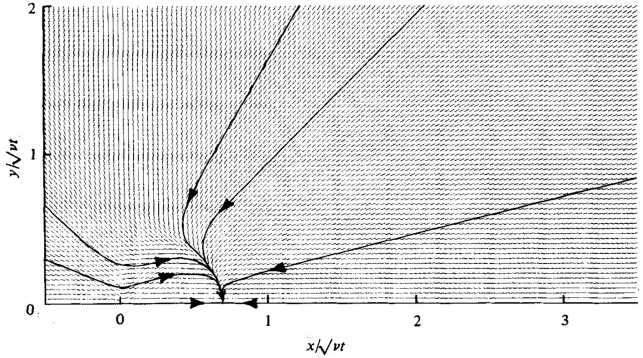

Re = 2

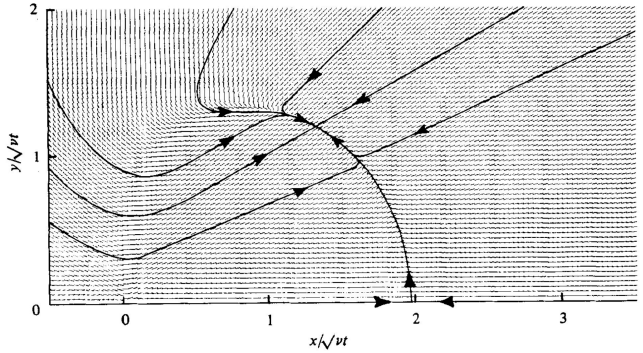

Re = 8

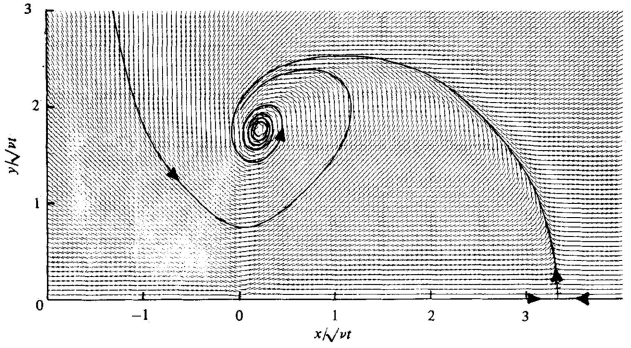

Re = 20

STANFORD
AERONAUTICS &
ASTRONAUTICS

Transition in the space of invariants Q_M and R_M

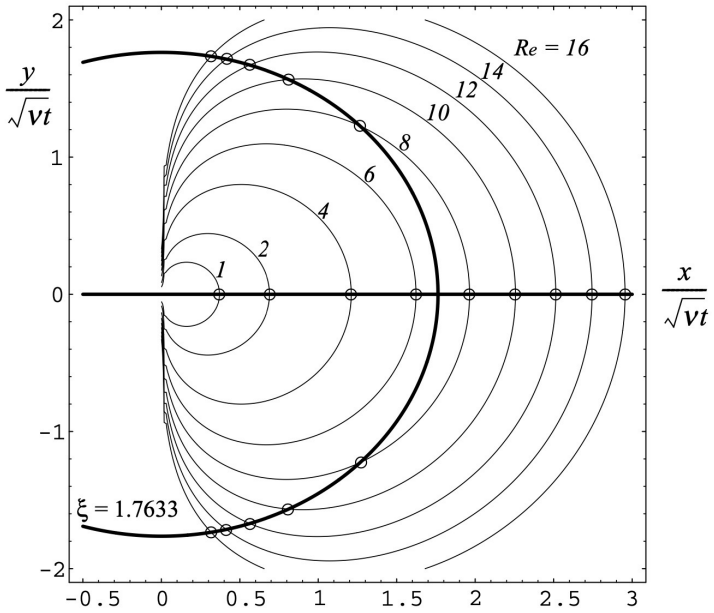

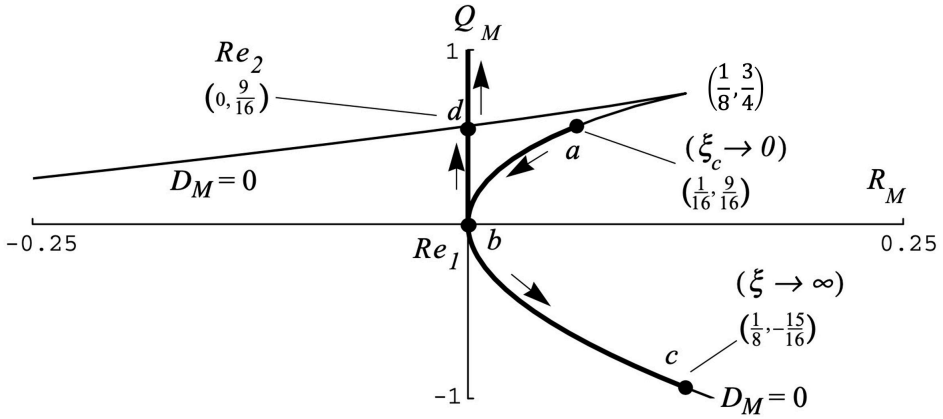

Fig. 11.7. Critical-point locations at several Reynolds numbers for the Stokes jet. The circle has radius 1.7633.

STANFORD AERONAUTICS & ASTRONAUTICS

Another view of particle paths in the Stokes jet.

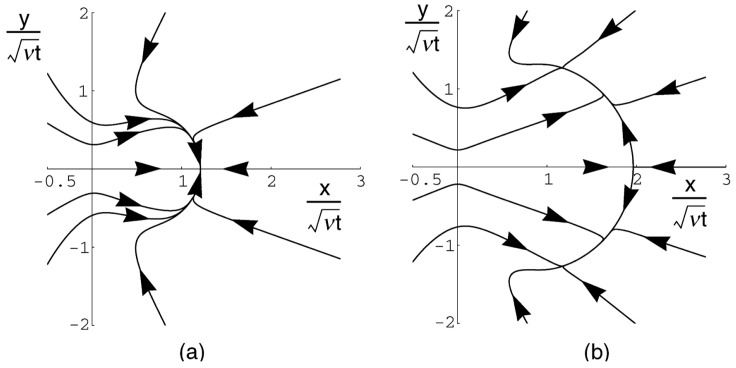

Fig. 11.9. Particle paths for the impulsively started creeping jet at (a) $Re = 4$ and (b) $Re = 8$.

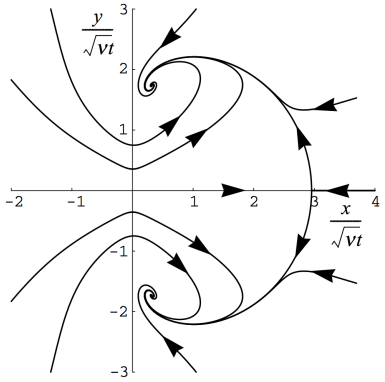

Fig. 11.10. Particle paths for the impulsively started creeping jet at $Re = 16$.

The impulsively started round jet undergoes a bifurcation in the phase portrait of particle paths. For the Stokes solution, the first transition to an off-axis stable node occurs at Re = 6.7806 and the onset of a starting occurs at Re=10.09089.

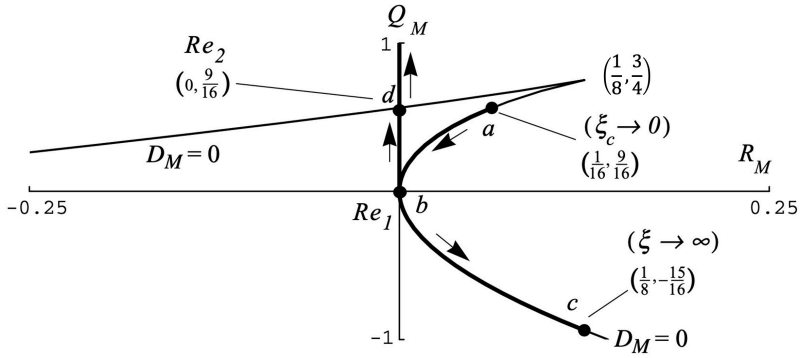

The nonlinear axisymmetric jet follows the same path in the space of Q_M and R_M invariants.

STANFORD
AERONAUTICS &
ASTRONAUTICS

Streamlines, vorticity and particle paths for the nonlinear round jet

Re=4 Re=6

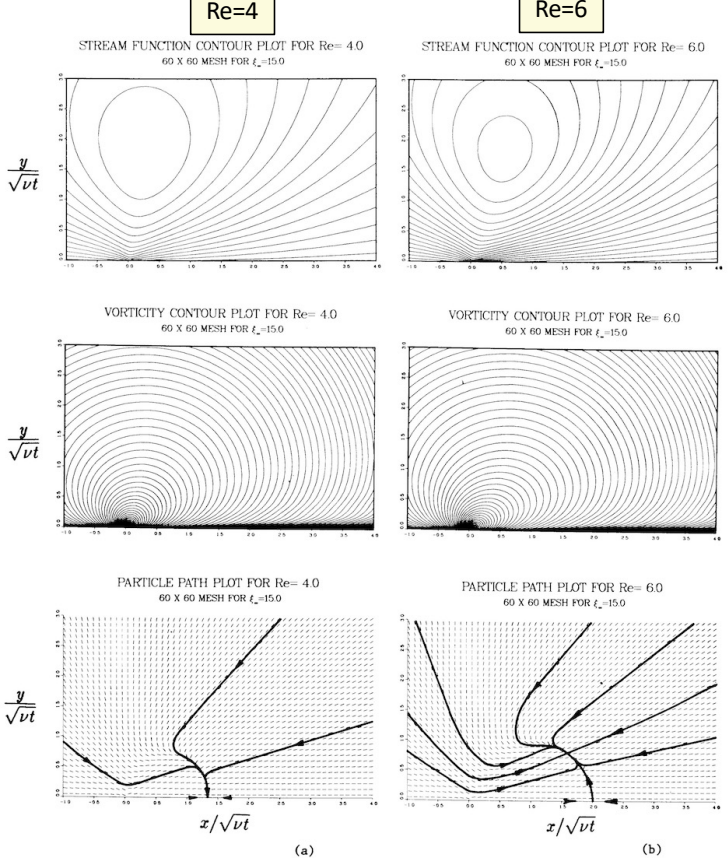

Figure 4. Computed solutions for the round jet at a) $Re = 4.0$ and b) $Re = 6.0$. Quantities displayed are self–similar stream function, vorticity and particle paths.

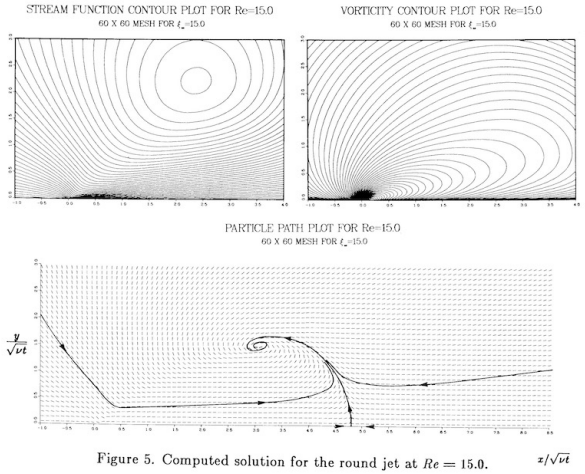

Re=15

Figure 5. Computed solution for the round jet at $Re = 15.0$.

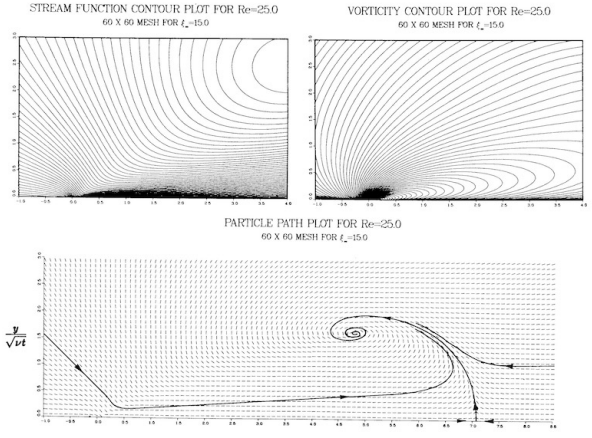

Re=25

Figure 6. Computed solution for the round jet at $Re = 25.0$.

STANFORD AERONAUTICS & ASTRONAUTICS

Invariance of the vector field of particle paths relative to a moving observer

The self-similarity in time of the jet enabled us to reduce the particle-path equations (11.83) to an autonomous system, (11.88). The invariance of the governing equations under the nonuniform translation group (11.14) can be used to show that, the vector field of particle paths in similarity coordinates is the same for all observers moving with the time scale appropriate to the flow. In Cartesian coordinates the equations for particle paths are

$$\frac{dx^i}{dt} = u^i[\boldsymbol{x}, t], \tag{11.125}$$

which, when transformed to similarity variables, become

$$\frac{d\xi^i}{d\tau} = U^i[\boldsymbol{\xi}] - \frac{1}{2}\xi^i, \tag{11.126}$$

where $\xi^i = x^i/(\nu t)^{1/2}$ and $\tau = \ln t$. In the round jet all length scales vary in proportion to $(\nu t)^{1/2}$. For an observer translating according to this function, the appropriate transformation of coordinates is

$$\begin{aligned}
\tilde{x}^j &= x^j + \alpha^j(\nu t)^{1/2}, \\
\tilde{t} &= t, \\
\tilde{u}^i &= u^i + \frac{\alpha^i}{2}\nu^{1/2}t^{-1/2}, \\
\frac{\tilde{p}}{\rho} &= \frac{p}{\rho} + x^k\frac{\alpha^k}{4}\nu^{1/2}t^{-3/2}, \quad \text{sum over } k
\end{aligned} \tag{11.127}$$

where the α^i determine the rate at which the observer moves in each of the three coordinate directions. In terms of similarity variables the transformation of velocities and coordinates, (11.127), becomes

$$\begin{aligned}
\tilde{\xi}^j &= \xi^j + \alpha^j, \\
\tilde{U}^i &= U^i + \frac{\alpha^i}{2}.
\end{aligned} \tag{11.128}$$

In contrast to the velocity vector field, the vector field of particle paths is invariant. To see this we transform the right-hand side of (11.126):

$$\tilde{U}^i - \frac{1}{2}\tilde{\xi}^i = \left(U^i + \frac{\alpha^i}{2}\right) - \frac{1}{2}(\xi^j + \alpha^j) = U^i - \frac{1}{2}\xi^j. \tag{11.129}$$

Because the α^i cancel all observers, moving or not, would assign the same numerical values to the components $d\xi^i, i = 1, 2, 3$, of the particle-path displacement vectors in similarity coordinates. A moving observer would assign these values at points that are uniformly displaced by a fixed amount $(\alpha^i\alpha^i)^{1/2}$ along a ray θ = constant, but this displacement does not affect the pattern of particle trajectories.

STANFORD
AERONAUTICS &
ASTRONAUTICS

Transition in the impulsively started jet describes the onset of a starting vortex

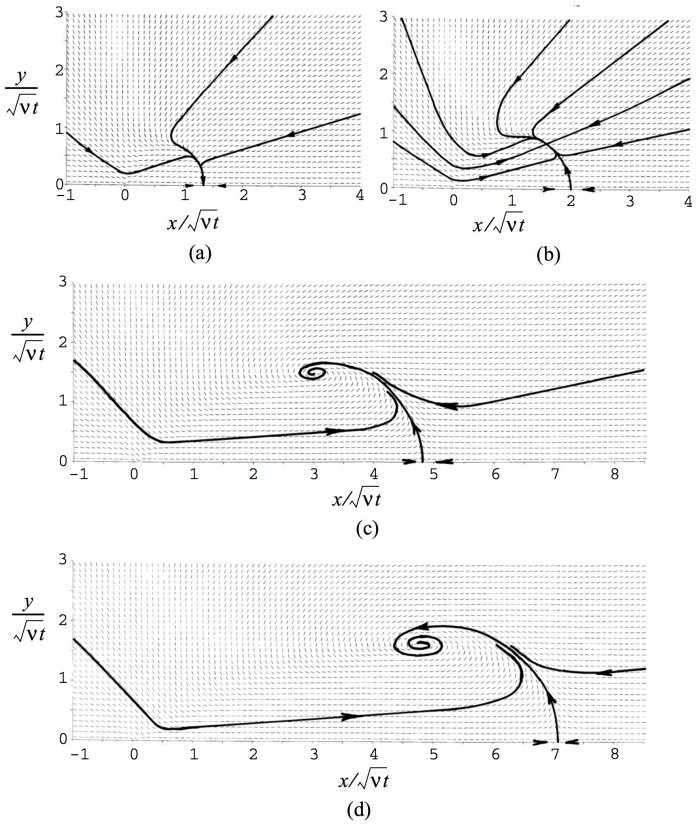

Fig. 11.11. Numerically computed particle paths in the round jet at Reynolds numbers (a) $Re = 4$, (b) $Re = 6$, (c) $Re = 15$, (d) $Re = 25$.

For the numerically computed nonlinear solution, the first transition to an off-axis stable node occurs at Re = 5.5 and the onset of a starting occurs at Re=7.545.

STANFORD
AERONAUTICS &
ASTRONAUTICS

Mixing of Material Lines at 3 Reynolds numbers

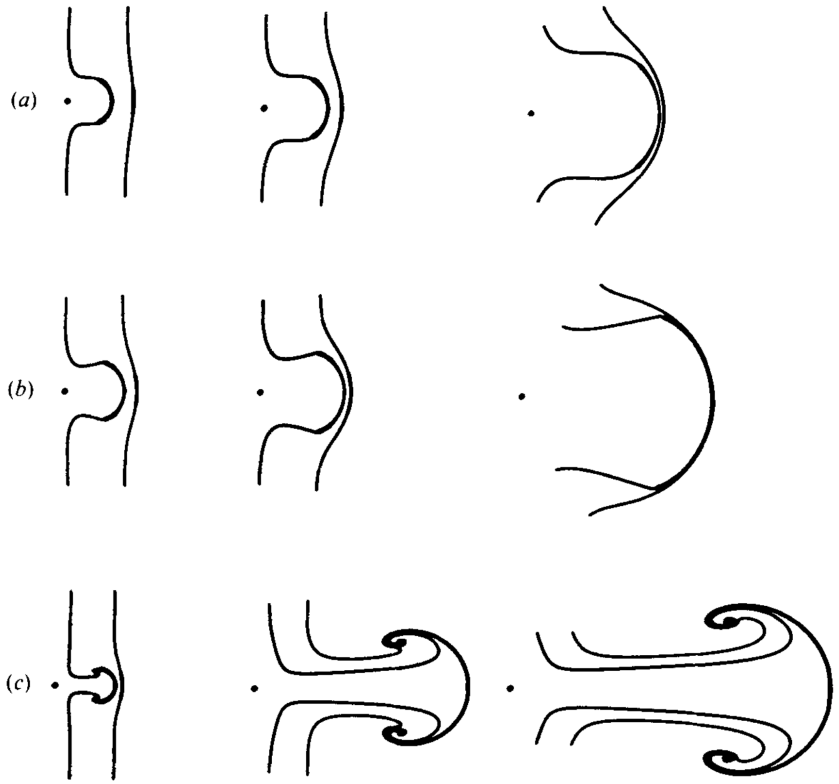

FIGURE 8. Distortion of timelines in physical coordinates under the action of the nonlinear round jet at (*a*) $Re = 4$, (*b*) $Re = 6$, (*c*) $Re = 30$. Time increases from left to right.

STANFORD
AERONAUTICS &
ASTRONAUTICS

Elliptic curves and 3-D flow patterns

STANFORD
AERONAUTICS &
ASTRONAUTICS

Use Q and R to study the local flow geometry of a temporally evolving mixing layer

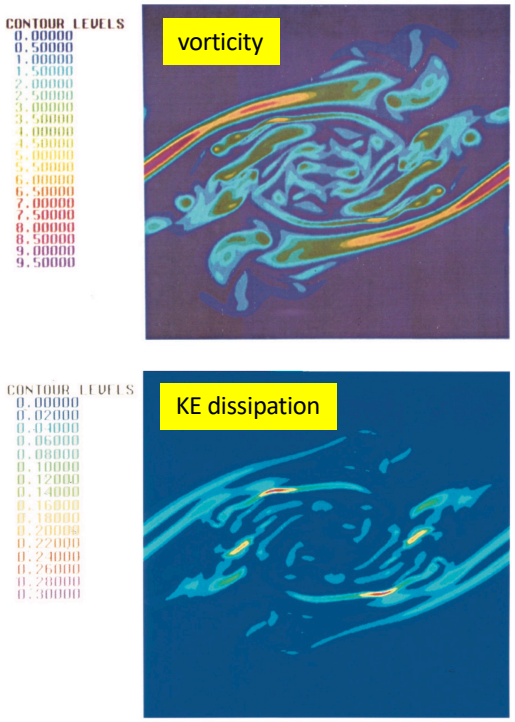

Color plate 1.

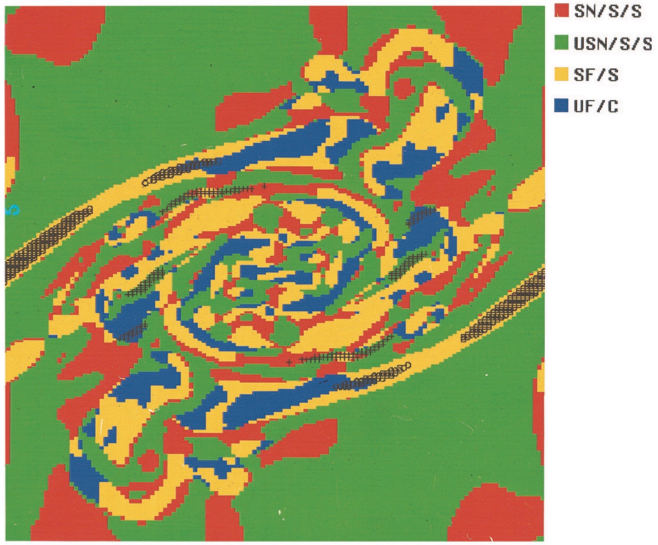

Color plate 2.

This is an efficient quantitative way to investigate the 3D structure of a turbulent flow.

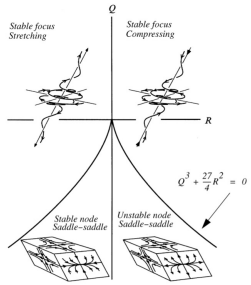

Fig. 3.9. Three-dimensional flow patterns in the plane $P = 0$ (from Reference [3.11]).

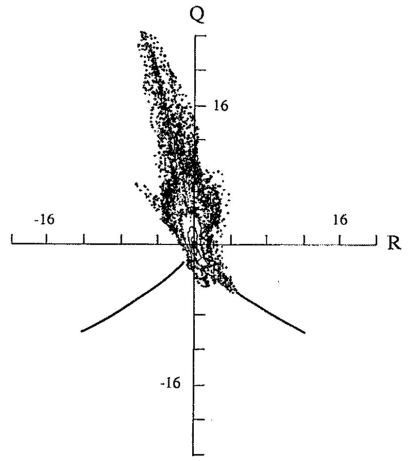

FIG. 2. Number density contour plot of velocity gradient tensor invariants from direct numerical simulation of a plane mixing layer by Moser and Rogers.[8] Dimensionless time $tU_0/\delta=29.8$ where δ is the initial vorticity thickness and U_0 is one-half the velocity difference across the layer. For further details see Ref. 5.

STANFORD AERONAUTICS & ASTRONAUTICS

Use the NS equations to analyze the dynamics of Q and R

Differentiate the NS equations to produce an equation for

$$\frac{\partial}{\partial x^j}\left(\frac{\partial u^i}{\partial t}+u^k\frac{\partial u^i}{\partial x^k}+\frac{1}{\rho}\frac{\partial p}{\partial x^i}-\nu\frac{\partial^2 u^i}{\partial x^k\,\partial x^k}\right)=0. \qquad (11.130)$$

Carrying out the differentiation and applying the continuity equation for incompressible flow, $a^i_i=0$, leads to

$$\frac{\partial a^i_j}{\partial t}+u^k\frac{\partial a^i_j}{\partial x^k}+a^i_k a^k_j+\frac{1}{\rho}\frac{\partial^2 p}{\partial x^i\,\partial x^j}-\nu\frac{\partial^2 a^i_j}{\partial x^k\,\partial x^k}=0. \qquad (11.131)$$

Now take the trace of (11.131) to generate the Poisson equation for the pressure:

$$\frac{1}{\rho}\frac{\partial^2 P}{\partial x^i\,\partial x^i}=-a^i_k a^k_i. \qquad (11.132)$$

Equation (11.132) is subtracted from (11.131) to make the pressure term trace-free. The final result is the transport equation for the velocity gradient tensor,

$$\frac{Da^i_j}{Dt}+a^i_k a^k_j-\frac{1}{3}\left(a^m_n a^n_m\right)\delta^i_j=h^i_j, \qquad (11.133)$$

where

$$h^i_j=-\frac{1}{\rho}\left(\frac{\partial^2 p}{\partial x^i\,\partial x^j}-\frac{1}{3}\frac{\partial^2 p}{\partial x^k\,\partial x^k}\delta^i_j\right)+\nu\frac{\partial^2 a^i_j}{\partial x^k\,\partial x^k}. \qquad (11.134)$$

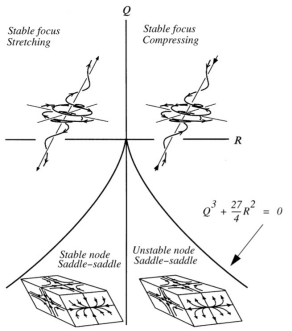

Fig. 3.9. Three-dimensional flow patterns in the plane $P=0$ (from Reference [3.11]).

$$Q=-\frac{1}{2}a^j_k a^k_j \qquad R=-\frac{1}{3}a^j_k a^k_m a^m_j$$

$$\frac{dQ}{dt}+3R=-a^i_k h^k_i \qquad \frac{dR}{dt}-\frac{2}{3}Q^2=-a^i_n a^n_m h^m_i$$

If $h^i_j=0$ the discriminant is conserved on particle paths.

$$D=Q^3+\frac{27}{4}R^2$$

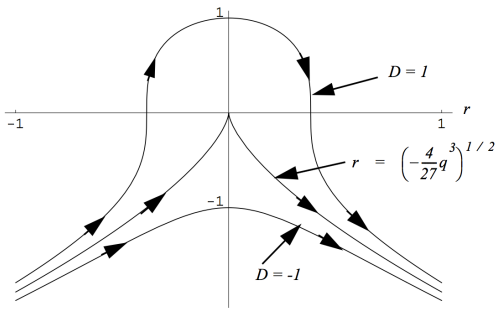

Fig. 6.6. Lines of constant normalized discriminant.

STANFORD
AERONAUTICS &
ASTRONAUTICS

Elliptic curves and 3-D flow patterns

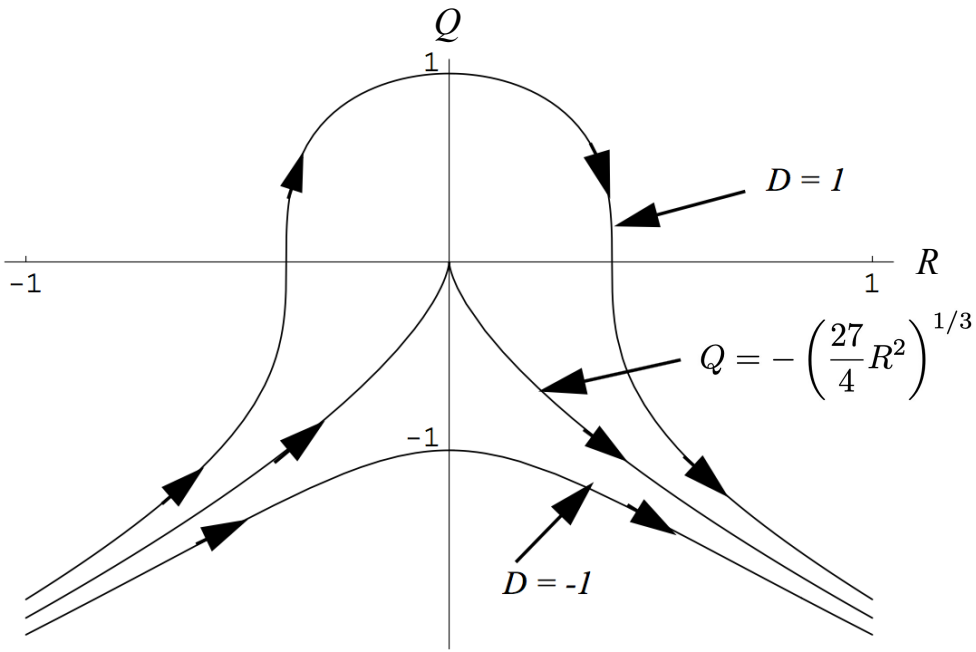

Fig. 6.6. Lines of constant normalized discriminant.

$$D = Q^3 + \frac{27}{4}R^2$$

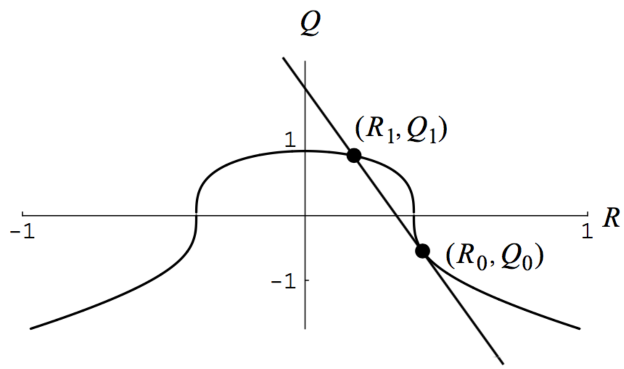

Fig. 6.7. Construction to find rational roots on a curve of constant D.

The cubic discriminant has the same value at both points of intersection in Figure 6.7,

$$Q_1^3 + \frac{27}{4}R_1^2 = Q_0^3 + \frac{27}{4}R_0^2, \tag{6.132}$$

and the straight line is of the form

$$R + aQ + b = 0. \tag{6.133}$$

At (R_0, Q_0) the straight line and line of constant D have the same slope as well as the same coordinates. This is used to evaluate a and b, and the equation of the straight line is determined to be

$$R + \left(\frac{2}{9}\frac{Q_0^2}{R_0}\right)Q + \left(-\frac{2}{9}\frac{Q_0^3}{R_0} - R_0\right) = 0. \tag{6.134}$$

Now evaluate (6.134) at (R_1, Q_1), and use it to replace R_1 in (6.132). The result

STANFORD
AERONAUTICS &
ASTRONAUTICS

is a cubic equation for Q_1, which can be factored as

$$(Q_1 - Q_0)^2 \left(Q_1 + \frac{1}{3}\frac{Q_0^4}{R_0^2} + 2Q_0 \right) = 0. \tag{6.135}$$

Two of the roots coincide with the tangent point. The third root, combined with (6.134), leads to the parameterization

$$\begin{aligned} Q_1 &= -\frac{1}{3}\frac{Q_0^4}{R_0^2} - 2Q_0, \\ R_1 &= \frac{2}{27}\frac{Q_0^6}{R_0^3} + \frac{2}{3}\frac{Q_0^3}{R_0} + R_0. \end{aligned} \tag{6.136}$$

It is clear that if Q_0 and R_0 are rational numbers, then so are Q_1 and R_1. Repeating the chord–tangent construction at the new root leads to a third rational root, and so on.

All the various bifurcations in the topology of the impulsively started round jet occur at rational values of the invariants of the velocity gradient tensor as well as the acceleration gradient tensor.

STANFORD
AERONAUTICS &
ASTRONAUTICS

Acceleration field in the round jet

When (11.133) is transformed to similarity variables for the round jet, the result is

$$-A^i_j + \left(U_k - \frac{1}{2}\xi_k\right)\frac{\partial A^i_j}{\partial \xi_k} + A^i_k A^k_j - \frac{1}{3}\left(A^m_n A^n_m\right)\delta^i_j = H^i_j, \quad (11.135)$$

where H is the same as (11.134) but expressed in terms of (U^i, P, ξ^i). At a critical point, the convective term in (11.135) is zero, and A and H are algebraically related by

$$-A^i_j + A^i_k A^k_j - \tfrac{1}{3}\left(A^m_n A^n_m\right)\delta^i_j = H^i_j. \quad (11.136)$$

Squaring (11.136) and taking the trace produces

$$Q_H = -\tfrac{1}{3}Q_A^2 + Q_A - 3R_A. \quad (11.137)$$

Cubing (11.136) and taking the trace produces

$$R_H = -R_A^2 - R_A + Q_A R_A - \tfrac{2}{3}Q_A^2 - \tfrac{2}{27}Q_A^3. \quad (11.138)$$

Now switch over, and square (11.138) and cube (11.137) to form the discriminant of the acceleration gradient tensor H: The result is

$$Q_H^3 + \tfrac{27}{4}R_H^2 = \left(Q_A^3 + \tfrac{27}{4}R_A^2\right)(1 + Q_A - R_A)^2. \quad (11.139)$$

A remarkably simple result! A generalization of this procedure is described in [11.27].

STANFORD
AERONAUTICS &
ASTRONAUTICS

We can express the invariants of H in terms of the invariants of M . The result is

$$\begin{aligned} Q_H &= 3Q_M - 3R_M - \tfrac{1}{3}Q_M^2 - \tfrac{27}{16}, \\ R_H &= -R_M^2 - \tfrac{9}{4}R_M + 2Q_M R_M - \tfrac{2}{27}Q_M^3 - \tfrac{5}{4}Q_M^2 + \tfrac{9}{4}Q_M - \tfrac{27}{32}, \\ Q_H^3 + \tfrac{27}{4}R_H^2 &= \left(Q_M^3 + \tfrac{27}{4}R_M^2 + \tfrac{27}{4}R_M\left(\tfrac{1}{2} - Q_M\right) - \tfrac{9}{16}Q_M^2\right)\left(R_M - \tfrac{3}{2}Q_M\right)^2. \end{aligned} \tag{11.140}$$

Note that the terms of sixth order in Q_A or Q_M that would be expected when the discriminant of H is formed in (11.139) and (11.140) have canceled. At the off-axis critical point in Figure 11.11, where $R_M = 0$ we find,

$$\begin{aligned} Q_H &= 3Q_M - \tfrac{1}{3}Q_M^2 - \tfrac{27}{16}, \\ R_H &= -\tfrac{2}{27}Q_M^3 - \tfrac{5}{4}Q_M^2 + \tfrac{9}{4}Q_M - \tfrac{27}{32}, \\ Q_H^3 + \tfrac{27}{4}R_H^2 &= \tfrac{9}{4}Q_M^4\left(Q_M - \tfrac{9}{16}\right). \end{aligned} \tag{11.141}$$

The trajectory of the critical points of the round jet in the (R_H, Q_H) plane, with the off-axis point parameterized by Q_M as in (11.141), is depicted in Figure 11.12. Four significant points are labeled in these plots:

STANFORD
AERONAUTICS & ASTRONAUTICS

Point a. This corresponds to the zero-Reynolds-number (Stokes flow) limit of the jet, where there is a single stable node on the jet axis. The invariants of this critical point are

$$(R_A, Q_A) = \left(\tfrac{1}{32}, -\tfrac{3}{16}\right),$$
$$(R_M, Q_M) = \left(\tfrac{1}{16}, \tfrac{9}{16}\right), \qquad (11.142)$$
$$(R_H, Q_H) = \left(-\tfrac{125}{2048}, -\tfrac{75}{256}\right).$$

Point b. Let the Reynolds number increase. At a critical Reynolds number of 5.5 the jet undergoes a bifurcation to a saddle on the jet axis and a stable node off the axis. The invariants at the bifurcation point are

$$(R_A, Q_A) = \left(\tfrac{1}{4}, -\tfrac{3}{4}\right),$$
$$(R_M, Q_M) = (0, 0), \qquad (11.143)$$
$$(R_H, Q_H) = \left(-\tfrac{27}{32}, -\tfrac{27}{16}\right).$$

Point c. As the jet Reynolds number increases to infinity, the on-axis critical point moves to infinity and the invariants asymptote to the values given at *c*:

$$(R_A, Q_A) = \left(\tfrac{27}{32}, -\tfrac{27}{16}\right),$$
$$(R_M, Q_M) = \left(\tfrac{1}{8}, -\tfrac{15}{16}\right), \qquad (11.144)$$
$$(R_H, Q_H) = \left(-\tfrac{9261}{2048}, -\tfrac{1323}{256}\right).$$

Point d. Above the first bifurcation Reynolds number, the invariants of the off-axis critical point move upward along a straight line until, at a second critical Reynolds number of 7.545, the off-axis critical point turns into a stable node. Thus a starting vortex from the jet is born. The invariants of the off-axis point at this Reynolds number are

$$(R_A, Q_A) = \left(-\tfrac{1}{32}, -\tfrac{3}{16}\right),$$
$$(R_M, Q_M) = \left(0, \tfrac{9}{16}\right), \qquad (11.145)$$
$$(R_H, Q_H) = \left(\tfrac{27}{2048}, -\tfrac{27}{256}\right).$$

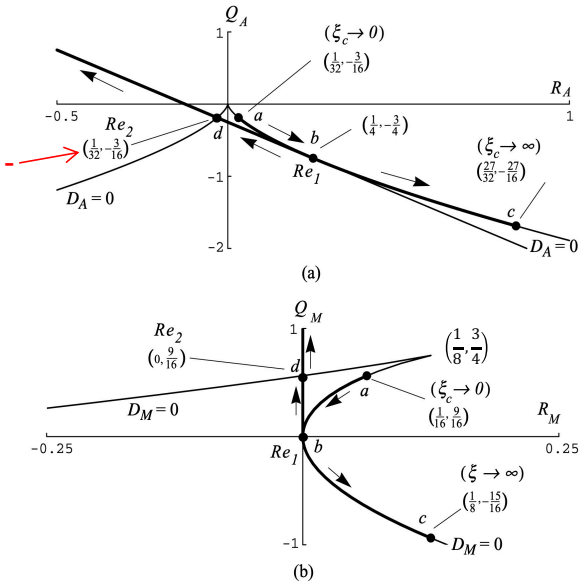

Fig. 11.8. Critical-point trajectories in the round jet: (a) the trajectory in (Q_A, R_A) coordinates at various Re; (b) the same trajectory in (Q_M, R_M).

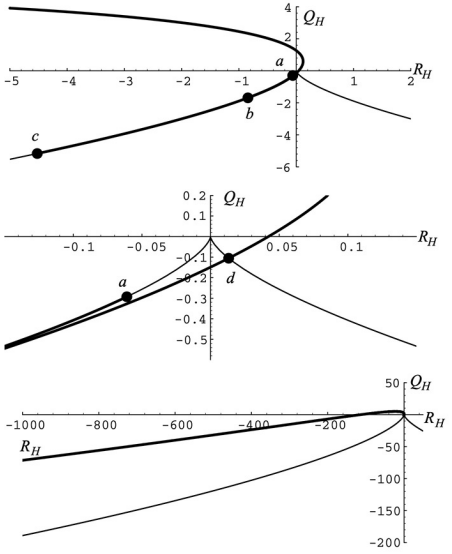

Fig. 11.12. Trajectory of the critical points of the round jet in the (Q_H, R_H) plane at three levels of magnification. Dots indicate several rational roots on the $D_H = 0$ boundary (on-axis critical point) and on the trajectory of the off-axis critical point. The labels *a*, *b*, *c*, and *d* coincide with the same labels in Figure 11.8.

These results have interesting implications for the limiting behavior of the off-axis critical point, which, eventually closes on the $D_H = 0$, $R_H < 0$ line as $Re \to \infty$. The signs of the discriminant of all three tensors are the same. Thus if M has complex eigenvalues, so have H and A. This means that the purely viscous, antisymmetric part of H^i_j remains important but diminishes compared to the symmetric pressure-dominated part as the Reynolds number increases. The viscous contribution to the forces at the critical point is never negligible. Finally, the invariants of the on-axis critical point have finite, rational values as the limit $Re \to \infty$ is taken. Few such infinite-Reynolds-number limits are known in fluid mechanics.

STANFORD
AERONAUTICS & ASTRONAUTICS

Contours of constant discriminant of the acceleration tensor $D_H=Q_H^3 + (27/4)\, R_H^2$

What trajectory in (Q_M, R_M) space would the critical point invariants of the 3D jet follow?

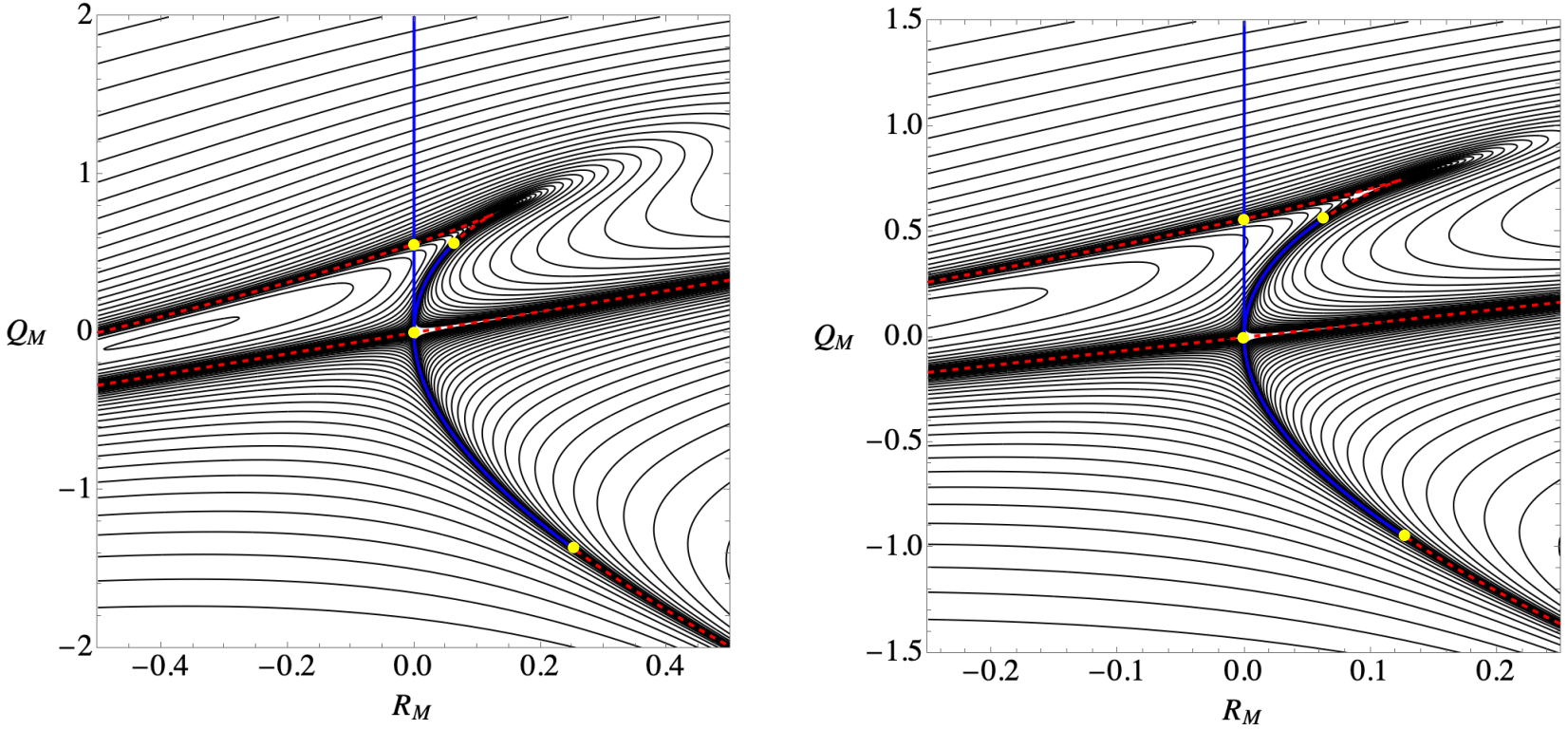

$$Q_H^3 + \tfrac{27}{4} R_H^2 = \left(Q_M^3 + \tfrac{27}{4} R_M^2 + \tfrac{27}{4} R_M\left(\tfrac{1}{2} - Q_M\right) - \tfrac{9}{16} Q_M^2\right)\left(R_M - \tfrac{3}{2} Q_M\right)^2$$

STANFORD
AERONAUTICS & ASTRONAUTICS

Generalization

Invariants of the velocity gradient tensor are evaluated at every grid point and placed on a cross plot of Q and R.

$$A_{ij}(t) = M_{ij} e^{\int f(t)dt}, \quad \frac{dA_{ij}}{dt} = A_{ij} f(t)$$

$$f A_{ij} + A_{ik}A_{kj} - 1/3(A_{mn}A_{nm})\delta_{ij} = H_{ij}$$

$$Q_H^3 + \tfrac{27}{4}R_H^2 = (Q^3 + \tfrac{27}{4}R^2)(R + fQ + f^3)^2$$

For the round jet the negative slope $f = -1$

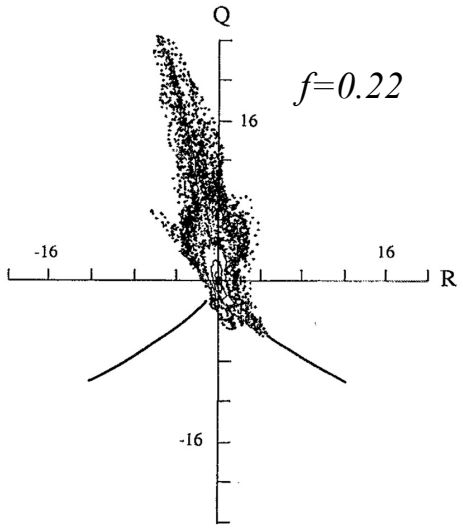

FIG. 2. Number density contour plot of velocity gradient tensor invariants from direct numerical simulation of a plane mixing layer by Moser and Rogers.[8] Dimensionless time $tU_0/\delta = 29.8$ where δ is the initial vorticity thickness and U_0 is one-half the velocity difference across the layer. For further details see Ref. 5.

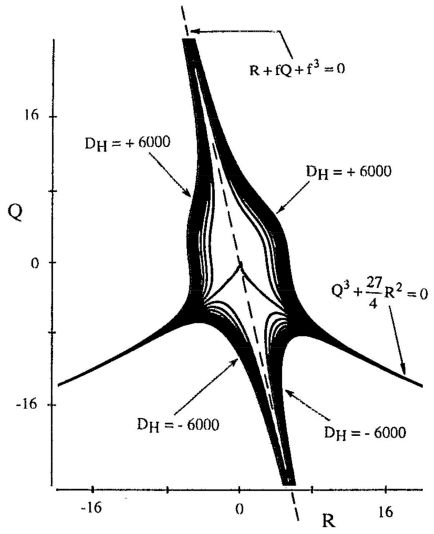

FIG. 3. Contours of constant $D_H = Q_H^3 + \frac{27}{4}R_H^2$ with $f(t) = 0.22$ [see Eq. (16)].

Cantwell, B. J. 1993. On the behavior of velocity gradient tensor invariants in direct numerical simulations of turbulence. *Phys. Fluids A* ***5 (8)***:2008–2013.

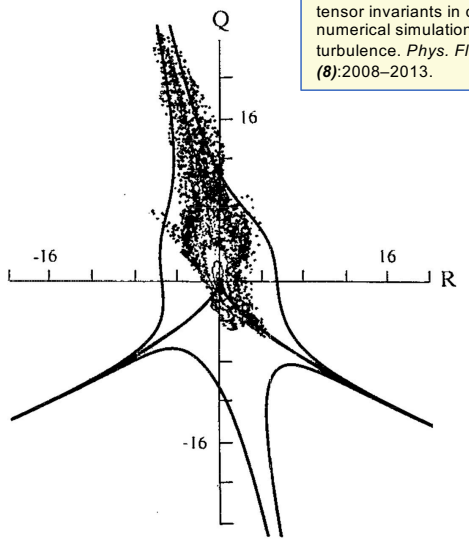

FIG. 4. Data from Fig. 2 superimposed on maximum, minimum, and zero contours of Fig. 3.

Previous numerical computations

Allen, G. A. and Cantwell, B. J. 1986. Transition and mixing in axisymmetric jets and vortex rings. NASA Contractor Report 3893.

Finite difference computation on a 60x60 mesh on a CDC7600

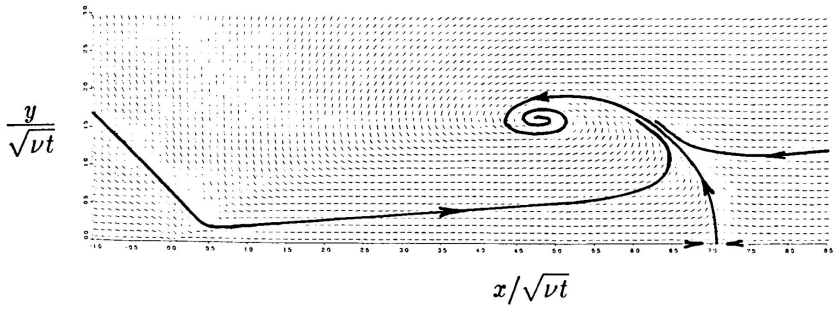

S. K. Stanaway, B. J. Cantwell, P. R. Spalart 1988. A Numerical Study of Viscous Vortex Rings Using a Spectral Method. NASA Technical Memorandum 101041.

Spectral computation of viscous interacting vortex rings using vector spherical harmonics

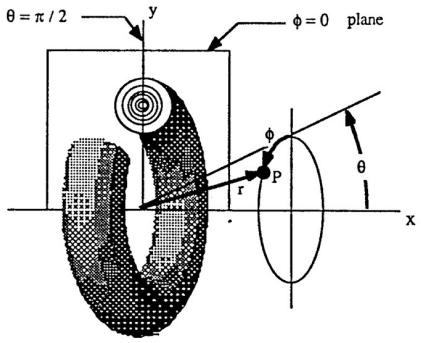

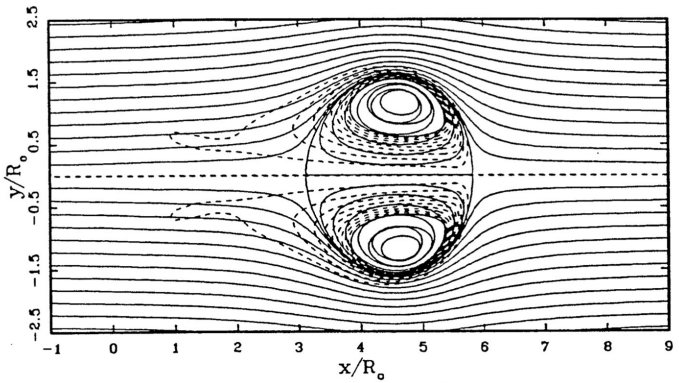

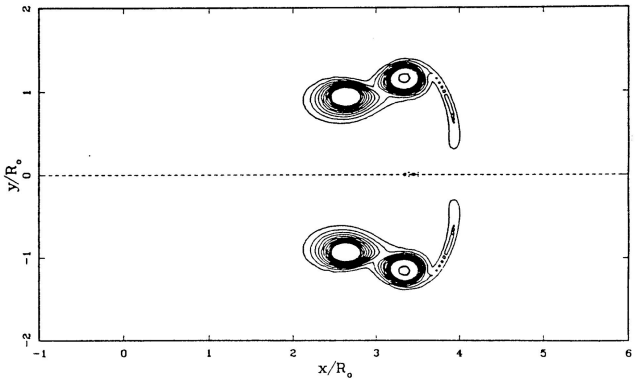

STANFORD AERONAUTICS & ASTRONAUTICS

Concluding Remarks

What is the trajectory of the fully 3-D jet in the space of (Q_M, R_M) invariants?

Presumably waves will form and associated with the waves will be 3D critical points, increasing in number as the Reynolds number is increased. What is the trajectory of the flow in the space of invariants, and can the infinite Reynolds number topological limit of the jet be inferred from a moderate Reynolds number computation? Can the onset of 3D flow be induced without permanently introducing a length scale to the flow?

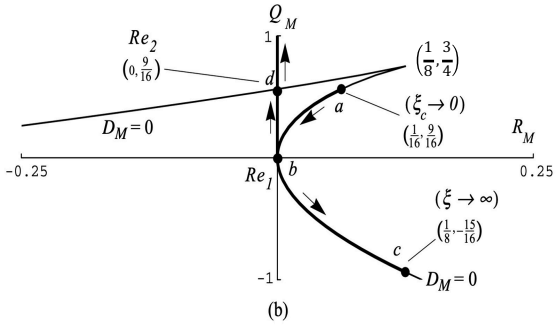

Fig. 11.8. Critical-point trajectories in the round jet: (a) the trajectory in (Q_A, R_A) coordinates at various Re; (b) the same trajectory in (Q_M, R_M).

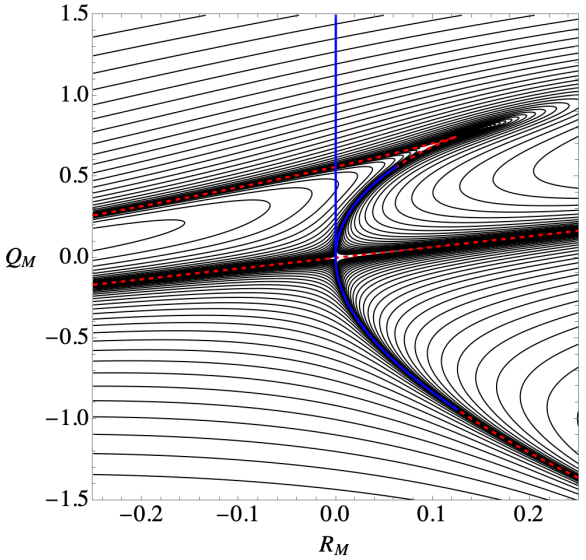

This problem, and perhaps others with k = ½, presents us with a unique opportunity to learn about the fundamentally geometric nature of turbulent flow in the limit of infinite Reynolds number.

STANFORD
AERONAUTICS &
ASTRONAUTICS

Main References

Cantwell, Brian J., *Introduction to Symmetry Analysis,* Cambridge University Press, Cambridge Texts in Applied Mathematics, 2002.

Cantwell, B. J. 1978. Similarity transformations for the two-dimensional unsteady stream-function equation. *J. Fluid Mech*. **85** (2):257–271.

Cantwell, B. J. 1986. Viscous starting jets. *J. Fluid Mech*. **173**:159–189.

Cantwell, B. J. 1981. Transition in the axisymmetric jet. *J. Fluid Mech*. **104**:369–386.

Chong, M. S., Perry, A. E., and Cantwell, B. J. 1990. A general classification of three-dimensional flow fields. *Phys. Fluids A* **2**:765–777.

Cantwell, B. J. 1992. Exact solution of a restricted Euler equation for the velocity gradient tensor. *Phys. Fluids A* ***4 (4)***: 782 - 793.

Cantwell, B. J. 1993. On the behavior of velocity gradient tensor invariants in direct numerical simulations of turbulence. *Phys. Fluids A* ***5 (8)***:2008–2013.

Landau, L. 1944. A new exact solution of the Navier–Stokes equations, *C. R. Acad. Sci. Dokl*. **43**:286–288.

Squire, H. B. 1951. The round laminar jet. *Q. J. Mech. Appl. Math*. **4**:321–329.

Allen, G. A. and Cantwell, B. J. 1986. Transition and mixing in axisymmetric jets and vortex rings. NASA Contractor Report 3893.

Cantwell, B. J. and Allen, G. A. 1983. Transition and mixing in impulsively started jets and vortex rings, in *Turbulence and Chaotic Phenomena in Fluids*, Proceedings of the IUTAM Symposium, Kyoto, Japan, edited by T. Tatsumi.

Cantwell, B. J. 2000. Elliptic curves and three-dimensional flow patterns. *Nonlinear Dynamics* **22**:29–38.

STANFORD
AERONAUTICS &
ASTRONAUTICS

Acceleration field in the round jet

Here some of the theory of elliptic curves and the development in Reference [11.28] will be used to explore the geometry of the forces at the critical points of the round jet. First we need to develop the transport equation for the velocity gradient tensor $a^i_j = \partial u^i/\partial x^j$ by taking the gradient of the Navier–Stokes equations,

$$\frac{\partial}{\partial x^j}\left(\frac{\partial u^i}{\partial t} + u^k\frac{\partial u^i}{\partial x^k} + \frac{1}{\rho}\frac{\partial p}{\partial x^i} - \nu\frac{\partial^2 u^i}{\partial x^k\,\partial x^k}\right) = 0. \tag{11.130}$$

Carrying out the differentiation and applying the continuity equation for incompressible flow, $a^i_i = 0$, leads to

$$\frac{\partial a^i_j}{\partial t} + u^k\frac{\partial a^i_j}{\partial x^k} + a^i_k a^k_j + \frac{1}{\rho}\frac{\partial^2 p}{\partial x^i\,\partial x^j} - \nu\frac{\partial^2 a^i_j}{\partial x^k\,\partial x^k} = 0. \tag{11.131}$$

Now take the trace of (11.131) to generate the Poisson equation for the pressure:

$$\frac{1}{\rho}\frac{\partial^2 P}{\partial x^i\,\partial x^i} = -a^i_k a^k_i. \tag{11.132}$$

Equation (11.132) is subtracted from (11.131) to make the pressure term trace-free. The final result is the transport equation for the velocity gradient tensor,

$$\frac{Da^i_j}{Dt} + a^i_k a^k_j - \frac{1}{3}\left(a^m_n a^n_m\right)\delta^i_j = h^i_j, \tag{11.133}$$

where

$$h^i_j = -\frac{1}{\rho}\left(\frac{\partial^2 p}{\partial x^i\,\partial x^j} - \frac{1}{3}\frac{\partial^2 p}{\partial x^k\,\partial x^k}\delta^i_j\right) + \nu\frac{\partial^2 a^i_j}{\partial x^k\,\partial x^k}. \tag{11.134}$$

When (11.133) is transformed to similarity variables for the round jet, the result is

$$-A^i_j + \left(U_k - \frac{1}{2}\xi_k\right)\frac{\partial A^i_j}{\partial \xi_k} + A^i_k A^k_j - \frac{1}{3}\left(A^m_n A^n_m\right)\delta^i_j = H^i_j, \tag{11.135}$$

where H is the same as (11.134) but expressed in terms of (U^i, P, ξ^i). At a critical point, the convective term in (11.135) is zero, and A and H are algebraically related by

$$-A^i_j + A^i_k A^k_j - \tfrac{1}{3}\left(A^m_n A^n_m\right)\delta^i_j = H^i_j. \tag{11.136}$$

Squaring (11.136) and taking the trace produces

$$Q_H = -\tfrac{1}{3}Q_A^2 + Q_A - 3R_A. \tag{11.137}$$

Cubing (11.136) and taking the trace produces

$$R_H = -R_A^2 - R_A + Q_A R_A - \tfrac{2}{3}Q_A^2 - \tfrac{2}{27}Q_A^3. \tag{11.138}$$

Now switch over, and square (11.138) and cube (11.137) to form the discriminant of the acceleration gradient tensor H: The result is

$$Q_H^3 + \tfrac{27}{4}R_H^2 = \left(Q_A^3 + \tfrac{27}{4}R_A^2\right)(1 + Q_A - R_A)^2. \tag{11.139}$$

A remarkably simple result! A generalization of this procedure is described in [11.27].

STANFORD
AERONAUTICS &
ASTRONAUTICS

This example of a temporally evolving mixing layer is similar to what I have in mind.

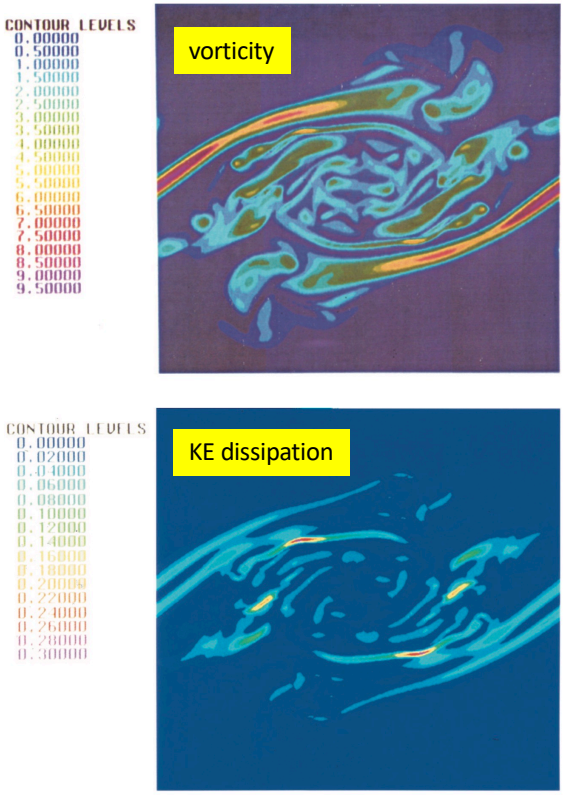

Color plate 1.

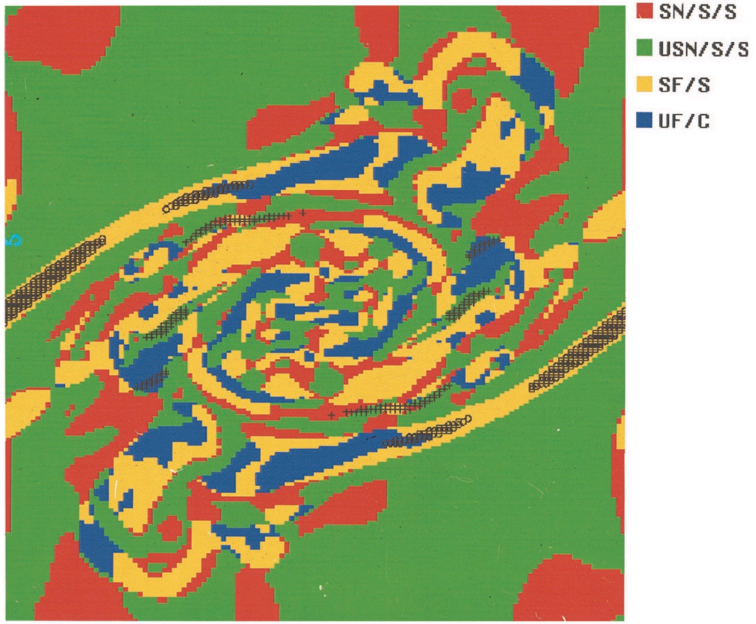

Color plate 2.

$$D = \frac{27}{4}R^2 + \left(P^3 - \frac{9}{2}PQ\right)R + Q^2\left(Q - \frac{1}{4}P^2\right)$$

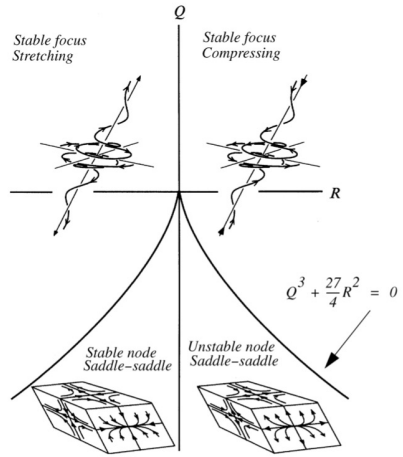

3.9. Three-dimensional flow patterns in the plane $P = 0$ (from Reference [3.11]).

This is a very useful and succinct way to investigate the 3D structure of a turbulent flow.